Molecular characterization of frog vocal neurons using constellation pharmacology

Ryota T. Inagaki[1], Shrinivasan Raghuraman[1], Kevin Chase[1], Theresa Steele[2], Erik Zornik[2], Baldomero Olivera[1], and Ayako Yamaguchi[1*]

[1]School of Biological Sciences, University of Utah, 257 South 1400 East, Salt Lake City, UT 84112-0840

[2]Biology Department, Reed College, Portland, Oregon 97202

*Correspondence:
Ayako Yamaguchi
a.yamaguchi@utah.edu

Keywords: constellation pharmacology, parabrachial nucleus, vocalizations, motor programs, premotor neurons

Abstract

Identification and characterization of neuronal cell classes in motor circuits are essential for understanding the neural basis of behavior. It is a challenging task, especially in a non-genetic model organism, to identify cell-specific expression of functional macromolecules. Here, we performed constellation pharmacology, calcium imaging of dissociated neurons to pharmacologically identify functional receptors expressed by vocal neurons in adult male and female African clawed frogs, *Xenopus laevis*. Previously we identified a population of vocal neurons called fast trill neurons (FTNs) in the amphibian parabrachial nucleus (PB) that express NMDA receptors and GABA and/or glycine receptors. Using constellation pharmacology, we identified four cell classes of putative fast trill neurons (pFTNs, responsive to both NMDA and GABA/glycine applications). We discovered that some pFTNs responded to the application of substance P (SP), acetylcholine (ACh), or both. Electrophysiological recordings obtained from FTNs using an *ex vivo* preparation verified that SP and/or ACh depolarize FTNs. Bilateral injection of ACh, SP, or their antagonists into PBs showed that ACh receptors are not sufficient but necessary for vocal production, and SP receptors play a role in shaping the morphology of vocalizations. Additionally, we discovered that the PB of adult female *X. laevis* also contains all the subclasses of neurons at a similar frequency as in males, despite their sexually distinct vocalizations. These results reveal novel neuromodulators that regulate *X. laevis* vocal production, and demonstrate the power of constellation pharmacology in identifying the neuronal subtypes marked by functional expression of cell-specific receptors in non-genetic model organisms.

New and Noteworthy

Molecular profiles of neurons are critical for understanding the neuronal functions, but their identification is challenging especially in non-genetic model organisms. Here, we characterized the functional expression of membrane macromolecules in vocal neurons of African clawed frogs, *Xenopus laevis*, using a technique called constellation pharmacology. We discovered that receptors for acetylcholine and/or substance P are expressed by some classes of vocal neurons, and their activation plays a role in the production of normal vocalizations.

Introduction

A major goal of neuroscience is to understand the neural basis of behavior. Identifying types of neurons in a neural circuitry underlying behavior is critical in achieving this goal. Among a variety of cellular classification techniques (e.g., morphological, physiological, anatomical, immunohistochemical), the molecular genetics approach has become a powerful tool in illuminating functional roles played by different classes of neurons in recent years. Neuron types defined either by gene expression during development (Goulding 2009; Grillner and Jessell 2009) and/or in adulthood (Haque et al. 2018) can be used to classify and test the functionality of neurons. For example, spinal interneurons marked by the expression of Shox2 but not of Chx10, and glutamatergic spinal interneurons marked by Hb9 expression both play roles in locomotor rhythm generation in mice (Caldeira et al. 2017; Dougherty et al. 2013), and GABAergic Maf-expressing interneurons regulate the speed of locomotion in *Drosophila* (Babski et al. 2019). However, the use of molecular genetics to identify types of neurons is challenging in non-genetic model organisms due to the limited availability of tools in these species. In this study, we applied a recently developed experimental approach called "constellation pharmacology" (Raghuraman et al. 2014) to characterize molecular profiles of neurons in the central vocal pathways of African clawed frogs, *Xenopus laevis*, a pseudotetraploid species with a long generation time that is challenging for genetic approach. In this technique, a series of target-selective pharmacological agents is applied to dissociated neurons while intracellular Ca^{2+} responses are monitored from ~1,000 neurons simultaneously; neurons can be classified into different classes based on unique combinations of functional receptors expressed by neurons.

Courtship vocalizations of a variety of vertebrate species are generated by central pattern generators (CPG) (Bass 2014; Konishi 2010; Sweeney and Kelley 2014), networks of neurons that generate rhythmic motor programs in the absence of rhythmic descending input or sensory feedback (Kiehn 2006; Marder and Bucher 2001). In this study, we identified the molecular profiles of neurons in the vocal CPG of *X. laevis* that offers advantages for the analyses of the neural basis of behavior due to its experimental amenability. Fictive vocalizations (i.e., rhythmic motor activity produced by an isolated brain preparation *ex vivo* that are facsimiles of neuronal activity generated during vocal production *in vivo*) can be readily and repeatedly elicited from the isolated brains of adult *X. laevis* in response to the application of serotonin (5-HT) (Rhodes et al. 2007). Using this preparation, we have previously identified a population of premotor neurons called fast trill neurons (FTNs) in the amphibian parabrachial nucleus (PB, previously labeled as the dorsal tegmental area of medulla, DTAM) that code for the duration and the rate of the male advertisement calls by driving laryngeal motor neurons (Zornik and Yamaguchi 2012). Based on whole-cell patch-clamp recordings obtained from FTNs, we identified that the neurons express NMDA receptors (NMDAR) and GABA and/or glycine (Gly) receptors (Lawton et al. 2017; Zornik and Yamaguchi 2012).

Using constellation pharmacology, we identified four subclasses of putative FTNs (pFTNs) based on their responsiveness to NMDA and GABA and/or Gly. We discovered that some of the pFTNs responded to acetylcholine (ACh) and/or substance P (SP). Although the involvement of these neuromodulators in vocal motor programs was previously unknown, electrophysiological recordings using the *ex vivo* preparation confirmed that FTNs indeed depolarize in response to the application of ACh and/or SP. Furthermore, bilateral injections of antagonists and agonists for ACh and SP into PBs revealed that ACh is necessary but not

sufficient for the vocal production, and SP plays a role in shaping the morphology of normal vocal motor programs. Furthermore, all subclasses of neurons identified in adult male PB are also present at a similar frequency in adult female PB even though vocalizations are sexually distinct in *X. laevis* (Kelley 1986). This study highlights the synergistic power of the constellation pharmacology and electrophysiological technique in identifying molecular profiles of neurons important for behavior in non-genetic model organisms.

Materials and Methods

Animals: Adult *Xenopus laevis* frogs (male, n=24, 4.5~7.2cm, 9.6~37.0g; female, n=5, 4.4~5.4cm, 11.0~18.2g) were obtained from NASCO. Sexually mature male *X. laevis* produce advertisement calls to attract females when they are sexually receptive, and adult females produce release calls to repel males when they are not sexually receptive. We ensured all the males and females used in the present study to be in the appropriate physiological state to produce advertisement or release calls, respectively. For males used in *ex vivo* whole-cell patch-clamp experiments and whole-brain fictive recording experiments, only the brains that generated fictive advertisement calls in response to the application of 5-HT were used. For the males used for the constellation pharmacology experiments, human chorionic gonadotropin was injected (hCG; Sigma-Aldrich) subcutaneously to bring them into sexual receptivity and vocalizations were recorded using hydrophones 1 to 7 days prior to the experiments; only the males that generated advertisement calls were used for the experiments. Females housed with other females in captivity remain sexually unreceptive. Therefore, for the constellation pharmacology experiments females that were not pre-treated with hCG were used. All the procedures were approved by the Institutional Animal Care and Use Committee at the University of Utah.

Primary culture of neurons: Animals were anesthetized with 1.3% tricaine methanesulfonate (MS222; 300-500µl; Sigma-Aldrich). Immediately after decapitation, the isolated skull was placed on a 100mm Petri dish filled with ice-cold frog saline (in mM: 103 NaCl, 13 $NaHCO_3$, 2 $CaCl_2$, 2 KCl, 0.5 $MgCl_2$, HEPES and 11 dextrose, pH7.8) oxygenated with 99% O_2 and 1% CO_2. A brain was dissected out from the skull, and all meninges were removed from the brain for slice preparation. The isolated brain was attached to a vibratome chamber filled with ice-cold saline, and sliced transversely (250~300µm in thickness), a protocol previously established for electrophysiological experiments (Yamaguchi et al. 2003). Under a stereomicroscope, PBs were visualized, and were cut out from the brain slice using a scalpel and transferred into a centrifuge tube with 1ml of frog saline. Neurons were dissociated first by placing the tissue in 2.5% Trypsin for 10 minutes, and washed three times with 5ml of Frog Neuronal Culturing Medium (FNCM; 49% Frog Culturing Ringer in mM: 115 NaCl, 1 Na-pyruvate, 2 $CaCl_2$, 2 KCl, 0.5 $MgCl_2$, 10 HEPES and 11 dextrose, 49% L-15 medium, 1% Fetal bovine serum, 1% Penicillin streptomycin, pH7.8). The tissue was then triturated with Pasteur pipet until the whole tissue was dissociated and the solution became translucent, centrifuged at 1100 rpm (136 G) for 10 minutes, and concentrated by removing the supernatant. A sterilized silicon ring (10mm silicon ring with a 3mm diameter hole in the center) was placed on the bottom of polylysine coated culture wells (Corning). Twenty-five to 30µl of the dissociated cell suspension was applied on the center of silicon rings, 1ml of FNCM was added to the culturing chamber in an hour, and the neurons were incubated overnight at 20 to 22°C. Although dissociated cells consist mostly of somata and short processes, functional receptors and ion channels specific for each cell types are known to be expressed by somata (Curtice et al. 2016; Imperial et al. 2014; Raghuraman et al. 2014; Teichert et al. 2014; Teichert et al. 2012).

160 Calcium imaging: Dissociated neurons were loaded with a FURA-2 dye (2.5μM, 700μl, 380nm
161 excitation/510nm emission) for at least 1 hour before the start of an imaging experiment. The
162 FURA-2 loaded cells were excited alternately with 340 nm and 380 nm light every 2 seconds,
163 and a video image was obtained. The ratio of fluorescent intensities measured at 510 nm
164 emission provides a relative measure of cytosolic calcium concentration $[Ca^{2+}]_i$ (Iredale and
165 Dickenson 1995). The 340/380 nm ratio of fluorescence intensity was calculated over time to
166 trace the relative shift of $[Ca^{2+}]_i$ for each cell. Cells exhibit variable capabilities to absorb
167 FURA-2, and thus, load unevenly. This resulted in heterogeneous baseline fluorescence among
168 cells. The use of ratiometric imaging allowed us to normalize the uneven loading of the cells,
169 and obtain measurements of the changes in the $[Ca^{2+}]_i$ within each cell in response to ligand
170 applications. We obtained recordings from 1~3 wells per animal, 574 to 1, 378 cells imaged per
171 well at 10x objective/magnification. Cells are defined as regions of interest (ROIs) using a
172 bright-field image. Traces are ratiometric values for each ROI in the series of images taken at 2-
173 second intervals over the time-frame of the experiment.
174 The concentration and abbreviation of pharmacological agents used for this study are
175 summarized in Table 1. For all experiments, 700μl of the pharmacological agents were applied
176 every 7 minutes. Each ligand was applied for 10s followed by three washes to clear the
177 pharmacological agent from the wells. The application of ligands was manual and the solutions
178 were aspirated using a vacuum pump controlled by a foot pedal.
179 All neurons that responded to GABA with glycine, and NMDA with D-serine were
180 considered to be putative FTNs (pFTNs) based on our previous electrophysiological recordings
181 obtained from the neurons using *ex-vivo* preparation; FTNs showed IPSPs during fictive vocal
182 productions, and when pharmacologically isolated from all chemical synapses by applying TTX,

183 the membrane potentials of FTNs oscillated in response to the application of NMDA (Zornik and
184 Yamaguchi 2012). Since IPSPs exhibited by FTNs could be mediated by GABA and/or glycine,
185 we used a combination of both to identify the putative FTNs.
186 Whole-cell patch-clamp electrophysiological recordings: Whole-cell patch-clamp recordings
187 were obtained from neurons in PB using a whole-brain, *ex vivo* preparation, as previously
188 described (Zornik and Yamaguchi 2012). Briefly, patch-clamp electrodes (6–10 MΩ) made
189 from thick-walled borosilicate capillary tubes (1.5 mm outer diameter; 0.86 mm inner diameter),
190 were used to blind search for FTN by advancing the pipette vertically into PB using a motorized
191 micromanipulator (MC1000e; Siskiyou). The cells were determined to be FTNs based on their
192 membrane potential activity (Fig 5A) synchronized with 5-HT-induced fictive fast trills.
193 Intracellular solution contained the following (in mM): 115 KCl, 2 $MgCl_2$, 2 EGTA, 10 HEPES,
194 2 MgATP, and 0.2 NaGTP, pH 7.4. Once FTN is identified, the neuron was pharmacologically
195 isolated from action potential-mediated synaptic inputs by applying 1μM of TTX to the whole
196 brain. ACh (1mM final concentration) or SP (1μM final concentration) was bath applied for 10
197 minutes to determine if the resting membrane potential of the neuron (averaged over 30 seconds)
198 change before, during, and after the application.
199 *Ex vivo*, isolated brain preparation, PB injections, and fictive vocal recordings: Fictive
200 vocalizations were elicited from the isolated brains of sexually mature adult males. Brains were
201 isolated as described above ("Primary culture of neurons" section), and gradually returned to
202 room temperature (22°C) over the next hour, and then transferred to a recording chamber
203 superfused with oxygenated saline at 100ml/hour.
204 Laryngeal nerve activity was recorded bilaterally using a suction electrode placed over
205 cranial nerve (N.) IX-X. Local field potential (LFP) recordings from PBs were obtained

206 bilaterally using a 1 MΩ tungsten electrode (FHC, Bowdoin, ME) to confirm the location of PBs
207 prior to injection. During the fast trill portion of the fictive advertisement call, PBs shows a
208 stereotyped baseline wave superimposed with ~60Hz phasic activity (Zornik and Yamaguchi
209 2012). Prior to the start of the experiment, 5-HT (Sigma, 30 μM, final concentration) was bath
210 applied to elicit fictive advertisement calls. To examine if substance P (SP) and acetylcholine
211 (ACh) are sufficient to elicit fictive vocalizations, 350nL of 1μM SP or ACh solution including
212 Texas Red dissolved in saline was injected into both PBs using Nanoject (Drummond Scientific)
213 at a rate of 10 nl/sec. It took a total of ~90 seconds to complete the bilateral injection; 35
214 seconds to inject into each PB, and up to 20 seconds to switch the injection pipette from one PB
215 to the other. Nerve recordings were obtained during the injection as well as for 5 minutes
216 following the injection. To determine if ACh and SP are necessary for the fictive vocal
217 production, a combination of atropine (1mM) and tubocurarine (1mM, both dissolved in saline,
218 including Texas Red) or aprepitant (a neurokinin-1 receptor antagonist, 0.4mM dissolved in 10%
219 DMSO in frog saline, including Texas Red) were injected bilaterally into PBs (350nL each)
220 using the methods described above, followed by the bath application of 5-HT within 10 seconds
221 of the completion of the injection. Five minutes after the injection and/or application of 5-HT,
222 superfusion was reinstated at the maximum rate (~10 ml/minute) for 5 minutes to wash out the 5-
223 HT, then at a slower rate (~125ml/hour) for one to four hours. To test the effects of the vehicles
224 on the PBs, the experiments were repeated using injections of vehicles alone (350nL of saline or
225 10% DMSO in saline at 10nL/sec on each side) followed by the bath application of 5-HT.
226 Except for ACh injection experiment (see Results section, Fig 6B), only brains that showed vocal
227 recovery following the experimental treatment were used for the analyses.

228 Nerve and LFP signals were amplified using differential amplifiers (Models 1700 and
229 1800, respectively; A-M Systems, Carlsborg, WA), and band-pass filtered (10 Hz – 5 kHz and
230 0.1 – 5 kHz, respectively). All signals were digitized at 10 kHz (Digidata 1440A; Molecular
231 Devices, Sunnyvale, CA), and recorded on a PC using Clampex software (Molecular Devices).
232 Histology: Brains injected with pharmacological agents were fixed with 4% paraformaldehyde
233 overnight at 4°C, placed into 30% sucrose solution for 24 hours, and horizontally sectioned into
234 30μm thickness using a freezing sliding microtome. Sections were counterstained using
235 neurotrace 500/525 (Thermofisher Scientific). Injection sites were photographed and analyzed
236 under an Olympus BX41 microscope with a digital camera (Retiga 2000R, QImaging, Surrey,
237 Canada).
238 Constellation pharmacology data analyses: For imaging experiments, ratiometric values are
239 indicators of internal calcium levels. The time-course of the ratio was analyzed using a set of
240 functions written in R (Team 2013). The maldiquant package (Gibb and Strimmer 2012) was
241 used to correct baselines, smooth, and detect peaks. All traces were baseline corrected using the
242 estimateBaseline function with the "SNIP" method and smoothed using the smoothIntensity
243 function with the "SavitzkyGolay" method and a half WindowSize of 3. Peaks were detected
244 using the detectPeaks function with the "MAD" method, a halfWindowSize of 30 and a SNR.lim
245 setting of 4. All ROIs were scored as yes/no response to each input based on the presence of a
246 peak in the response window of 30 seconds following the application of pharmacological agents.
247 Thresholds were established to define possible peaks in the response window. We used a signal
248 to noise ratio (SNR) threshold of 4 with at least a value above the baseline threshold of .05 to
249 control for false-positive in regions of very low variance in recordings. These threshold values

give a false-positive rate < 0.001 (e.g. peaks during times of no input). Traces with obvious abnormal response patterns were removed from the analysis.

Fictive vocalizations data analyses:

The bath application of 5-HT to the brains bilaterally injected with aprepitant into the parabrachial nucleus elicited fictive advertisement calls with abnormal morphology in terms of the amplitude and the frequency of the compound action potentials (CAPs). To quantitatively compare the morphology of the fictive advertisement calls produced in the presence and absence of aprepitant, we measured the peak amplitude and the instantaneous frequency (i.e., reciprocal of the inter-CAP interval) of the CAPs generated before, during, and after (vehicle alone) the injection of aprepitant and plotted it against the order of the CAPs. Three to 10 calls were sampled from each experimental condition of each animal, and cross-correlation coefficients of the peak amplitude and instantaneous frequency profile of the calls were calculated from all pair-wise combinations (i.e., n*(n-1)/2 for each condition, where n stands for the total number of songs sampled for each condition from each animal). The average and the standard deviation of cross-correlation coefficients were calculated for each experimental condition in each animal. High coefficients close to 1 indicate more stereotyped call morphology.

Results

Monitoring intracellular calcium in live parabrachial neurons

Although culturing neurons of adult vertebrate animals has been difficult (Eide and McMurray 2005), we were able to obtain healthy dissociated cell cultures of optimal density (885 $\pm$ 222 cells per culturing chamber, mean $\pm$ standard deviation, n=17 chambers) from adult

parabrachial (PB) nucleus as shown in Figure 1A. The optimization of dissociation protocol, attachment substrates, and culture media, are described in detail in the Materials and Methods section. Figure 1B and C show fluorescence images from the same field of view as shown in the bright-field image in Figure 1A. Pseudocolored ratiometric images of $[Ca^{2+}]_i$ are acquired at rest (Fig 1B) and are monitored continuously for the duration of the experiment. Fig 1C shows the image acquired when the high extracellular concentration of KCl (30mM, high $[K^+]_o$) stimulus elicited an increase in $[Ca^{2+}]_i$ in a subset of cells. Because the expression of voltage-gated Ca^{2+} channels is seen in neurons but not in glial cells (Carmignoto et al. 1998), increased $[Ca^{2+}]_i$ in response to high $[K^+]_o$ was taken as a proxy for neurons. Among all dissociated cells, 85.0 $\pm$ 6.7% (mean $\pm$ standard deviation, n=8) of cells were classified as neurons; the proportion of neurons among all dissociated cells was consistent across individuals, as evident in the small value of the standard deviation.

Classification of PB neurons using constellation pharmacology

Once the neurons were distinguished from glial cells among all dissociated PB cells with high $[K^+]_o$, we serially applied a panel of pharmacological agents and monitored $[Ca^{2+}]_i$ responses from ~500 to 1,000 dissociated neurons simultaneously. Activation of receptors that depolarize the membrane potentials, which in turn increase the conductance of voltage-gated Ca^{2+} channels, were observed as increases in $[Ca^{2+}]_i$. In contrast, activation of GABA and/or Gly receptors that hyperpolarize the membrane potentials were deduced indirectly using the following method. High $[K^+]_o$ was applied three times with 7 minutes intervals and Ca^{2+} signals obtained from these three applications were compared (Fig 2). Between the first and the second high $[K^+]_o$ exposure, the cells were incubated with the combination of GABA and Gly. If the

296 cells express GABA and/or Gly receptors, the second high $[K^+]_o$ results in either reduced or no
297 Ca^{2+} signals due to the increased influx of I_{Cl}^- that counteracts the membrane depolarization. The
298 recovery of the calcium signal on the 3rd high $[K^+]_o$ is used as a control to verify that the
299 reduction/elimination of Ca^{2+} signals during the 2nd high $[K^+]_o$ was due to the GABA and Gly
300 application and not due to general deterioration of the health or desensitization of the cells (Fig
301 2).

302 In addition to two ligand groups that are known or suspected to elicit responses from the
303 FTNs (NMDA with D-serine, GABA with glycine), we tested if 5-HT, a neurotransmitter that
304 initiates fictive vocalizations, modulate the excitability of the FTNs. Furthermore, we selected
305 five additional ligands (histamine, bradykinin, acetylcholine, substance P, and ATP) that are
306 known to be involved in regulating respiratory rhythms in the brainstem (Doi and Ramirez 2008;
307 Funk 2013; Raghuraman et al. 2014; Ramirez et al. 2018; Shao and Feldman 2009) to classify
308 FTNs. The vocal neural circuitry is considered to have evolutionarily originated from the
309 respiratory neural circuitry (Bass and Baker 1997), and thus, we hypothesized that there is a
310 significant overlap in receptors expressed by the respiratory and vocal neural circuitry.
311 Histamine and bradykinin, however, elicited responses from very few dissociated *X. laevis* PB
312 neurons (2.5 $\pm$ 0.05% and 2.5 $\pm$ 0.70% of all neurons, mean $\pm$ standard deviation, respectively,
313 n=2). Thus, we focused on the remaining 6 ligand groups to classify FTNs (Table 1, four of the
314 ligands, NMDA with D-serine and GABA with Gly, were co-applied as pairs). It should be
315 noted that, although the combination of GABA and Gly were applied to dissociated cells in most
316 experiments, we discovered in a separate experiment (n=3) that PB cells sensitive to a cocktail of
317 GABA and Gly responded to GABA alone (34 $\pm$ 15%), to Gly alone (1 $\pm$ 1%), or to both (65 $\pm$

318 14%), indicating that about 99% of PB neurons that show inhibitory responses express GABA
319 receptors, two-third of which additionally express Gly receptors.

320 Representative calcium imaging traces obtained from two PB neurons are shown in
321 Figure 2. Figure 2A shows a Ca^{2+} profile of two neurons that responded to high $[K^+]_o$, but not to
322 any other pharmacological agents. Figure 2B exemplifies a type of neuron that responded to the
323 NMDA with D-serine, SP, ACh, ATP, and GABA with Gly (the neuron on top trace responded
324 to 5-HT in addition). These traces reveal that the two groups of neurons have a distinct
325 combination (constellation) of membrane receptors, and thus can be classified as two distinct
326 types.

327 To classify cell types contained in the PB of male *X. laevis*, we first used both cell size
328 and Ca^{2+} profile in response to a high $[K^+]_o$, and ATP to subdivide neurons into two major
329 classes, A and B (see below). The sizes of the dissociated PB neurons were heterogeneous,
330 consistent with our previous observations in brain slice and fixed brain preparations (A.
331 Yamaguchi unpublished data). Neuron classes A and B were further divided into subclasses
332 based on their response profile to a series of agonists (Table 2).

333 Class A cells (Table 2) are defined as neurons with a surface area >100μm² (Table 2, Fig
334 3A left) with the following response property; they exhibit transient $[Ca^{2+}]_i$ increase in response
335 to ATP with the peak amplitude larger than those in response to high $[K^+]_o$ (Fig 3B). Class A
336 cells constitute 17 ± 3% (n=8) of all dissociated cells obtained from male *X. laevis*. Although all
337 class A cells responded to ATP, they responded differently to other agonists, and can be divided
338 further into five subclasses based on their response profile (Table 2). Although some class A
339 cells showed responses to NMDA with D-Ser or to GABA with Gly application (Table 2), none
340 of the cells responded to both. Thus, class A cells were ruled out from being putative FTNs.

Class B cells are defined as neurons with a surface area <150μm² (Fig 3A) with a transient $[Ca^{2+}]_i$ increase with a peak amplitude in response to a repeated application of high $[K^+]_o$ consistently higher than those in response to any other ligands (Fig 3C). Class B cells constitute the majority of dissociated PB cells in males (68 ± 4%, n=8). The class B cells can be further divided into seven subclasses (Table 2), four of which responded to both NMDA with D-ser and GABA with Gly, a response profile consistent with FTNs. Thus, we considered these subclasses of neurons as putative FTNs (pFTNs), and investigated them further. Figure 4 shows the examples of calcium imaging traces obtained from all four subclasses of pFTNs (pFTNs I through IV) in response to the application of an array of ligands. Although 5-HT is potent in eliciting fictive vocalizations, the proportion of pFTNs that responded to 5-HT was relatively low (9 – 20 %, Table 2). In addition, responses to ATP was also low and variable (14 – 42%, Table 2). Thus, the responsiveness to these two ligands was not used to categorize subclasses of pFTNs (Table 2). Four subclasses of pFTNs exhibited the following response profiles. The most common subclass, pFTN-I (30 ± 3% of all dissociated neurons, n=8), did not respond to substance P (SP) nor acetylcholine (ACh, Fig 4A, Table 2). The second most frequent subclass, pFTN-II (11 ± 1%, n=8) responded to SP (Fig 4B, Table 2). The third most common subclass, pFTN-III (5 ± 1%, n=8), responded to ACh (Fig 4C, Table 2). The least common subclass, pFTN IV (3 ± 1%, n=8), responded to both SP and ACh (Fig 4D, Table 2).

Validating *in vitro* findings in intact circuits

Among four subclasses of pFTNs, three showed responsiveness to ACh, SP, or both. To determine if FTNs are indeed sensitive to ACh and/or substance P, we carried out whole-cell patch-clamp recordings from FTNs in an *ex vivo*, whole-brain preparation. After FTNs were

functionally identified based on the firing patterns during fictive advertisement calls elicited in response to the bath application of 5-HT (Fig 5A), the neurons were pharmacologically isolated from action potential-mediated synaptic inputs by applying 1μM TTX to the whole brain, and the changes in the membrane potential were measured in response to the bath application of ACh (1mM) or SP (1μM) in a current-clamp mode (Fig 5B). The results showed that 3 out of 4 FTNs depolarized in response to both ACh and SP, and the remaining 1 neuron depolarized only in response to ACh (Fig 5C). All of the neurons hyperpolarized after the ligands are washed out from the bath (Fig 5B, C). The results confirmed that FTNs in intact circuits indeed express ACh and NK-1 receptors, and are likely to include pFTN III and IV.

Role of substance P and acetylcholine in fictive vocalizations

If FTNs depolarize in response to SP and ACh, what are the functions of these neurotransmitters in the vocal pathways of male *X. laevis*? We first examined if SP and ACh are *sufficient* to elicit fictive advertisement calls by injecting SP (1 μM) or ACh (1 mM) bilaterally into PBs (350nL into each side) using an *ex vivo* whole-brain preparation while recordings were obtained from the laryngeal motor nerves (n = 4 for SP, n = 8 for ACh). By including Texas Red in the injection solution, the targeting of PBs was confirmed histologically *post hoc* (Fig 6A). The results showed that the bilateral injection of ACh into PBs failed to elicit fictive advertisement calls in all the brains, although tonic activity was recorded from the laryngeal motor nerves during the injection in some brains (Fig 6C middle trace). After 1 to 4 hours of wash, none of the ACh injected brains generated fictive advertisement calls in response to the bath application of 5-HT (Fig 6C right trace). In contrast, brains (n=6) that received bilateral saline (vehicle) injection of the same volume (350 nL) into PBs generated fictive calls in

response to the bath application of 5-HT after 1 to 2 hours of wash (data not shown). The results indicate that the lack of vocal recovery in ACh-injected brains are not due to any mechanical damage incurred to the PBs, but due to a long-lasting inhibitory effect of ACh on the central vocal pathways. In contrast, bilateral injections of SP into PBs (n=4) resulted in the variable outcome; one brain generated fast trills (Fig 6D1), another brain produced slow trills (Fig 6D2), and the two remaining brains generated no fictive vocalizations even though the bath application of 5-HT after 1 to 2 hours of wash elicited fictive vocalizations (Fig 6D3). The bath application of ACh (1mM) and SP (1μM) mirrors the PB injection results; the bath application of ACh (n = 3) did not elicit fictive vocalizations from any of the isolated brains, whereas the bath application of SP (n=7) elicited fictive advertisement call from one brain, fictive slow trills from three brains, and no calls from the remaining three brains (data not shown). The brains that did not sing in response to the bath application of ACh and SP generated fictive vocalizations in response to 5-HT 1 to 2 hours after the wash, indicating that these brains were capable of generating fictive vocalizations. Given that the concentrations of the bath applied ACh and SP are the same as those that depolarize the membrane potential in the previous whole-cell patch-clamp recordings using the same *ex vivo* preparation (Fig 5C), the results suggest that the depolarization of FTNs by ACh is not sufficient to elicit fictive vocalizations, and the excitation of FTNs by SP can activate the vocal CPG in some brains but its potency is lower than that of 5-HT.

Next, we examined if these two neurotransmitters are *necessary* for the activation of the vocal pathways. To this end, a combination of atropine (a muscarinic ACh receptor antagonist, 1mM) and tubocurarine (a nicotinic ACh receptor antagonist, 1mM) or aprepitant (a neurokinin-1 receptor antagonist, 0.4mM) were injected bilaterally (350nL each) into PBs just before 5-HT was applied to the bath (n = 5 for atropine/tubocurarine, n = 3 for aprepitant). When 5-HT was

410 applied to the brain that received bilateral injections of atropine/tubocurarine, none of the brains
411 generated fictive advertisement calls (Fig 6E middle panel). All brains produced fictive calls in
412 response to 5-HT prior to the atropine/tubocurarine injection (Fig 6E left panel). One hour after
413 the atropine/tubocurarine injection, when a vehicle (saline, 350nL each) was injected bilaterally
414 into the PBs of the same brains followed by 5-HT application, fictive advertisement calls were
415 elicited from all the brains (Fig 6E right panel). The results suggest that the activation of nAChR
416 and/or mAChR of in PB neurons is necessary for vocal production in male *X. laevis*. In contrast,
417 5-HT application preceded by the bilateral injection of aprepitant did not block fictive
418 vocalizations in any of the brains, although the morphology of 5-HT induced fictive calls were
419 abnormal (Fig 6F middle panel). The progressive increase in rate and amplitude of compound
420 action potentials (CAPs), hallmarks of fast trills (Fig 6C through F left panel, Fig 6G left graphs),
421 were absent from the fictive calls produced by brains injected with aprepitant; the CAP repetition
422 rates were either set at fast (~60Hz, n=2) or slow rate (~30Hz, n=1, Fig 6G), and the CAP
423 amplitude was variable (Fig 6G middle graphs). The application of 5-HT into brains injected
424 with vehicle alone into PB (350nL 10% DMSO) one hour after the aprepitant injection produced
425 stereotypical fictive calls with progressive increase in the amplitude and the rate (Fig 6G right
426 graphs). When the cross-correlation coefficients of the CAP amplitude and the CAP
427 instantaneous frequency of fictive advertisement calls were calculated, fictive calls before the
428 aprepitant injection and those elicited with the vehicle injection showed high cross-correlation
429 coefficients (amplitude; 0.901 ± 0.003, 0.786 ± 0.063, instantaneous frequency; 0.859 ± 0.046,
430 0.776 ± 0.078, mean $\pm$ standard deviation for control and vehicle injection), whereas the calls
431 with aprepitant injection showed low cross-correlation coefficients (0.423 ± 0.134, 0.426 ± 0.143
432 for amplitude and instantaneous frequency). The results show that the aprepitant injection in PB

433 blocked the progressive increase in the CAP rates and amplitude, and the loss of stereotypy of
434 the fictive advertisement calls, suggesting that the SP in PB plays a role in shaping the
435 morphology of fast trills.
436
437 **Comparison of male and female PB neurons.**
438 Male and female *X. laevis* produce sexually distinct vocalizations to coordinate
439 reproduction. A non-gravid female clasped by a male produces the release calls that are made of
440 a series of clicks repeated at 6 to 10Hz, much slower than those of males (Kelley et al. 2017).
441 Local field potential recordings obtained from the PB of female brains during fictive release calls
442 show very little vocal-related activity (A. Yamaguchi and E. Zornik, unpublished observations).
443 However, the application of testosterone to adult females masculinizes their vocalization within
444 5 to13 weeks (Potter et al. 2005), and their PBs show strong vocal-related activity during fictive
445 advertisement calls (A. Yamaguchi and E. Zornik, unpublished observations). To determine if
446 the types and frequency of vocal neurons contained in PB are distinct in the sexes, we compared
447 the types of PB neurons obtained from male and sexually unreceptive female *X. laevis*.
448 Surprisingly, all of the classes and subclasses (listed in Table 2) of PB neurons including all
449 pFTNs identified in males were also found in the dissociated PB cells from sexually unreceptive
450 female *X. laevis* (Fig 7 A-D). Furthermore, the frequency of all the neuron subclasses, including
451 pFTNs, did not differ significantly from between the sexes (Figure 8). The results suggest that
452 despite distinct vocalizations produced by the sexes, the PBs of males and females contain
453 neurons with similar molecular profiles at a similar frequency.
454
455

Discussion

The results of the present study (1) revealed previously unknown receptors expressed by the functionally salient vocal neurons, fast trill neurons (FTNs), (2) discovered the involvement of the newly identified receptors in vocal production, and (3) identified the similarity in the types and frequency of neurons contained in the vocal nuclei of the sexes despite the sexually distinct vocalizations. The study showcases a powerful methodology for molecular characterization of neurons constituting neural circuitry in all organisms, and thus signifies a major step forward in addressing unique questions presented by non-genetic model organisms.

Using constellation pharmacology, parabrachial (PB) neurons of adult male *X. laevis* were classified. We identified two major classes, A and B, that were further subdivided into a total of 12 subclasses based on their unique response profiles to ligands. In particular, four subclasses of neurons in B class were identified as putative FTNs because of their sensitivity to both NMDA and GABA/glycine, characteristics of FTNs previously identified electrophysiologically (Lawton et al. 2017; Zornik and Yamaguchi 2012). Three of the four putative FTNs (pFTN-II, III, and IV) responded to acetylcholine (ACh) and/or substance P (SP), neurotransmitters whose involvement in the brainstem central vocal pathways were previously unknown. Further electrophysiological experiments obtained from the confirmed FTNs using *ex vivo* preparation showed that the application of ACh and/or SP to synaptically isolated FTNs indeed depolarize the membrane potentials of FTNs, confirming the prediction derived from the results of constellation pharmacology. Whether the sensitivity to NMDA and GABA is unique to the FTNs within the *X. laevis* PB is currently not known, and thus neurons classified as putative FTNs in this study may have included non-FTNs. Despite this challenge, we were able to identify two additional neuromodulators that modify the membrane potential of the FTNs.

These results demonstrate the power of constellation pharmacology together with electrophysiology in identifying key functional molecules expressed by neurons in neural circuitry.

We further tested the roles of the SP and ACh in the vocal productions using *ex vivo* preparations. Bilateral injection of ACh into PBs (Fig 6C) or its bath application to the isolated brains (Fig 6B) never elicited fictive vocalizations from any of the brains, whereas bilateral injection of SP into PBs (Fig 6D) or its bath application (Fig 6B) elicited fictive vocalizations from about half of the brains. The results suggest that the depolarization of the FTNs by ACh is not sufficient in generating fictive vocalizations, and the potency of SP-mediated FTN activation in eliciting fictive vocalizations is low. In contrast, injection of the antagonists for acetylcholine receptors (AChR) in PBs blocked the 5-HT induced vocal production (Fig 6E), and the injection of neurokinin-1 receptor (NK-1R) antagonist into PBs resulted in 5-HT induced vocalizations with abnormal morphology (Fig 6F, G). Thus, the AChR and NK-1R expressed by FTNs play an important role in mediating/modulating vocal production.

One caveat in interpreting the results of the series of pharmacological experiments is as follows. Among dissociated PB neurons, there are subclasses of cells other than pFTNs that respond to ACh and/or SP (Table 2). Thus, the injection of ACh, SP, or their antagonists did not selectively modulate the FTNs, but all PB neurons with the appropriate receptors. Nonetheless, our inability or limited ability to elicit fictive vocalizations with ACh and SP, either by bilateral injection into PBs (Fig 6B, C) or by bath application, is in stark contrast to reliable and repeated activation of fictive vocalizations in response to the bath application of 5-HT, suggesting activation of FTNs by ACh and SP were insufficient in eliciting fictive vocalizations reliably.

One interesting observation we made was that once ACh is injected bilaterally into the PBs, following applications of 5-HT after up to four hours of wash never elicited fictive vocalizations (Fig 6B, C). This was not the case when ACh was applied to the bath (Fig 6B); the brains responded to the following 5-HT applications by generating fictive calls after 1 to 2 hours of wash. These results may be explained by the internalization or desensitization of cholinergic receptors in PB neurons when they are exposed to a high concentration of the agonists (Giniatullin et al. 2005; Lambert et al. 2018; Wan et al. 2015). The brains that received ACh injections in the PBs may have lost functional cholinergic receptors in PB for a prolonged period of time, and thus have become essentially the same as those that received atropine and tubocurarine injections in the PBs and lost their ability to generate fictive vocalizations in response to 5-HT. The experience-dependent change in the availability of cholinergic receptors in PB should be tested in the future to determine the validity of the speculation.

Previously, we demonstrated that fictive vocalizations are elicited by activating 5-HT_{2C} receptors expressed either in the rostral raphe nucleus, the laryngeal motor nucleus, or both (Yu and Yamaguchi 2010). Although the receptors critical for the call initiation may not be expressed by the FTNs, we hypothesized that FTNs may express other types of 5-HT receptors that contribute to the vocal rhythm generations. However, our results showed that the FTNs do not express 5-HT receptors. Together with the results that show that the depolarization of FTNs by SP and ACh is not sufficient to initiate fictive vocalizations reliably, we suggest that FTNs are a part of the vocal rhythm generator that is downstream of the population of 5-HT_{2C}R-positive neurons in the rostral raphe nucleus and/or laryngeal motor nucleus that are responsible for the vocal initiation.

523 Do NK-1R and AChR also play a role in the activation of the vocal CPGs in other
524 species? Brainstem vocal circuits are known to play a critical role in vocal patterning in a
525 variety of vertebrate species (Hage and Jurgens 2006; Jurgens 2002; Rubsamen and Betz 1986;
526 Schmidt et al. 2012). Although the involvement of AChR in vocal productions have been
527 identified in the forebrains and midbrains of birds, primates, rats, and cats (Brudzynski 2009;
528 Jurgens and Lu 1993; Meng et al. 2017; Silkstone and Brudzynski 2020), roles for AChR and
529 NK-1R in the vertebrate brainstem vocal pathways have not been described. It is possible that
530 NK-1R and AChR may have been re-purposed from the neurons contained in the parabrachial
531 nucleus, and/or the brainstem respiratory neural pathways. Both NK-1R and AChR are
532 expressed by neurons in PB of other vertebrate species. For example, muscarinic AChR is found
533 in the PB of cats (Mallios et al. 1995), rats (Christie and North 1988), and in Kölliker-Fuse
534 nucleus (one of the subdivisions within PB) in goats (Bonis et al. 2010), and NK-1 receptors are
535 found in PB of mice (Boscan et al. 2005). In addition, the activation of NK-1 or ACh receptors
536 of neurons in pre-Bötzinger Complex in mice and the paratrigeminal respiratory group of
537 lampreys can enhance respiratory rhythms (Cinelli et al. 2013; Del Negro et al. 2005; Mutolo et
538 al. 2011; Shao et al. 2008). Based on the embryonic origin, vocal CPGs of vertebrates are
539 hypothesized to have evolved from respiratory CPGs located in the brainstem (Bass and Baker
540 1997). Thus, ACh and NK-1 receptors expressed by FTNs may have derived from the pre-
541 existing PB neurons or the neurons in the brainstem respiratory pathways, become adapted to
542 generate vocalizations through evolution.
543
544 Male and female *X. laevis* generate sexually distinct vocalizations. Surprisingly, the
545 female PB contained all the classes and subclasses of neurons identified in males at similar

546 frequencies. It is possible that male and female neurons classified as the same pFTN in this
547 study may actually be differentiated by sex-specific receptors and ion channels that were not
548 tested in this study. Single-cell RNA sequencing of male and female pFTNs will allow us to
549 address this question in the future. Nonetheless, there is some evidence suggesting that
550 functional neural circuitry underlying male-specific sexual behavior is present in the female CNS
551 while the mechanisms to activate the circuitry are absent in females. In mice and *Drosophila*, for
552 example, it has been shown that functional neural circuitries for male-specific courtship behavior
553 remain latent in the female brains and can be activated with experimental manipulation, even
554 though females never expressed male-specific courtship behavior *in vivo* throughout their lives
555 (Clyne and Miesenbock 2008; Kimchi et al. 2007; Rezaval et al. 2016). Interestingly, in *X.*
556 *laevis*, the administration of testosterone to adult females results in vocal masculinization in a
557 relatively short amount of time (5 to 13 weeks (Potter et al. 2005)). As in mice and *Drosophila*,
558 female *X. laevis* may be equipped with an array of latent neurons including FTNs responsible for
559 male-specific vocal behavior that can be unmasked in the presence of high levels of plasma
560 testosterone.
561
562 In this study, we used an integrated approach to identify receptors expressed by neurons
563 critical for the production of vocal behavior. We identified potential receptors expressed by the
564 dissociated neurons using constellation pharmacology, confirmed the functional expression of
565 the receptors by the vocal neurons using whole-cell patch-clamp recordings, and characterized
566 the functional roles played by the receptors expressed by the vocal neurons in generating
567 vocalizations using pharmacology and electrophysiology. This powerful approach is not limited
568 to genetic model organisms, but can be applied to any organisms, extending the horizon for

research to non-genetic model organisms that present unique and important questions in the field of neuroscience.

Author Contributions

R.T.I., S.R., B.O., and A.Y. developed the main idea, R.T.I., S.R., T.S., E.Z., and A.Y. conducted experiments, R.T.I., S.R., T.S., E.Z., A.Y., and K.C. analyzed the data, and R.T.I. and A.Y. wrote the paper with inputs from S.R., K.C. and E.Z.

Conflict of Interest

The authors declare that the research was conducted in the absence of any commercial or financial relationships that could be construed as a potential conflict of interest.

Funding

This work was supported by NSF IOS 1557945, 1934386 (AY), NSF IOS 1755423 (EZ), NIH NS091977 (EZ), and NIH GM48677 (BO).

Data Availability

The data that support the findings of this study are available from the corresponding author upon reasonable request.

References

Babski H, Jovanic T, Surel C, Yoshikawa S, Zwart MF, Valmier J, Thomas JB, Enriquez J, Carroll P, and Garces A. A GABAergic Maf-expressing interneuron subset regulates the speed of locomotion in Drosophila. *Nature communications* 10: 4796, 2019.

Bass AH. Central pattern generator for vocalization: is there a vertebrate morphotype? *Current opinion in neurobiology* 28: 94-100, 2014.

Bass AH, and Baker R. Phenotypic specification of hindbrain rhombomeres and the origins of rhythmic circuits in vertebrates. *Brain, behavior and evolution* 50 Suppl 1: 3-16, 1997.

Bonis JM, Neumueller SE, Krause KL, Kiner T, Smith A, Marshall BD, Qian B, Pan LG, and Forster HV. A role for the Kolliker-Fuse nucleus in cholinergic modulation of breathing at night during wakefulness and NREM sleep. *Journal of applied physiology (Bethesda, Md : 1985)* 109: 159-170, 2010.

Boscan P, Dutschmann M, Herbert H, and Paton JF. Neurokininergic mechanism within the lateral crescent nucleus of the parabrachial complex participates in the heart-rate response to nociception. *J Neurosci* 25: 1412-1420, 2005.

Brudzynski SM. Medial cholinoceptive vocaliation strip in the cat and rat brains: initiation of defensive vocalizations. In: *Handbook of mammalian vocalization An integrative neuroscience approach*, edited by Brudzynski SMAcademic Press, 2009, p. 265-280.

Caldeira V, Dougherty KJ, Borgius L, and Kiehn O. Spinal Hb9::Cre-derived excitatory interneurons contribute to rhythm generation in the mouse. *Scientific reports* 7: 41369, 2017.

Carmignoto G, Pasti L, and Pozzan T. On the role of voltage-dependent calcium channels in calcium signaling of astrocytes in situ. *J Neurosci* 18: 4637-4645, 1998.

Christie MJ, and North RA. Agonists at mu-opioid, M2-muscarinic and GABAB-receptors increase the same potassium conductance in rat lateral parabrachial neurones. *British journal of pharmacology* 95: 896-902, 1988.

Cinelli E, Robertson B, Mutolo D, Grillner S, Pantaleo T, and Bongianni F. Neuronal mechanisms of respiratory pattern generation are evolutionary conserved. *J Neurosci* 33: 9104-9112, 2013.

Clyne JD, and Miesenbock G. Sex-specific control and tuning of the pattern generator for courtship song in Drosophila. *Cell* 133: 354-363, 2008.

Curtice KJ, Leavitt LS, Chase K, Raghuraman S, Horvath MP, Olivera BM, and Teichert RW. Classifying neuronal subclasses of the cerebellum through constellation pharmacology. *J Neurophysiol* 115: 1031-1042, 2016.

Del Negro CA, Morgado-Valle C, Hayes JA, Mackay DD, Pace RW, Crowder EA, and Feldman JL. Sodium and calcium current-mediated pacemaker neurons and respiratory rhythm generation. *J Neurosci* 25: 446-453, 2005.

Doi A, and Ramirez JM. Neuromodulation and the orchestration of the respiratory rhythm. *Respiratory physiology & neurobiology* 164: 96-104, 2008.

Dougherty KJ, Zagoraiou L, Satoh D, Rozani I, Doobar S, Arber S, Jessell TM, and Kiehn O. Locomotor rhythm generation linked to the output of spinal shox2 excitatory interneurons. *Neuron* 80: 920-933, 2013.

Eide L, and McMurray CT. Culture of adult mouse neurons. *BioTechniques* 38: 99-104, 2005.

Funk GD. Neuromodulation: purinergic signaling in respiratory control. *Comprehensive Physiology* 3: 331-363, 2013.

Gibb S, and Strimmer K. MALDIquant: a versatile R package for the analysis of mass spectrometry data. *Bioinformatics (Oxford, England)* 28: 2270-2271, 2012.
Giniatullin R, Nistri A, and Yakel JL. Desensitization of nicotinic ACh receptors: shaping cholinergic signaling. *Trends in neurosciences* 28: 371-378, 2005.
Goulding M. Circuits controlling vertebrate locomotion: moving in a new direction. *Nature reviews Neuroscience* 10: 507-518, 2009.
Grillner S, and Jessell TM. Measured motion: searching for simplicity in spinal locomotor networks. *Current opinion in neurobiology* 19: 572-586, 2009.
Hage SR, and Jurgens U. On the role of the pontine brainstem in vocal pattern generation: a telemetric single-unit recording study in the squirrel monkey. *J Neurosci* 26: 7105-7115, 2006.
Haque F, Rancic V, Zhang W, Clugston R, Ballanyi K, and Gosgnach S. WT1-Expressing Interneurons Regulate Left-Right Alternation during Mammalian Locomotor Activity. *J Neurosci* 38: 5666-5676, 2018.
Imperial JS, Cabang AB, Song J, Raghuraman S, Gajewiak J, Watkins M, Showers-Corneli P, Fedosov A, Concepcion GP, Terlau H, Teichert RW, and Olivera BM. A family of excitatory peptide toxins from venomous crassispirine snails: using Constellation Pharmacology to assess bioactivity. *Toxicon : official journal of the International Society on Toxinology* 89: 45-54, 2014.
Iredale PA, and Dickenson JM. Measurement of intracellular free calcium ion concentration in cell populations using fura-2. *Methods in molecular biology (Clifton, NJ)* 41: 203-213, 1995.
Jurgens U. A study of the central control of vocalization using the squirrel monkey. *Medical engineering & physics* 24: 473-477, 2002.
Jurgens U, and Lu CL. Interactions between glutamate, GABA, acetylcholine and histamine in the periaqueductal gray's control of vocalization in the squirrel monkey. *Neuroscience letters* 152: 5-8, 1993.
Kelley DB. Neuroeffectors for vocalization in Xenopus laevis: hormonal regulation of sexual dimorphism. *Journal of neurobiology* 17: 231-248, 1986.
Kelley DB, Elliott TM, Evans BJ, Hall IC, Leininger EC, Rhodes HJ, Yamaguchi A, and Zornik E. Probing forebrain to hindbrain circuit functions in Xenopus. *Genesis (New York, NY : 2000)* 55: 2017.
Kiehn O. Locomotor circuits in the mammalian spinal cord. *Annual review of neuroscience* 29: 279-306, 2006.
Kimchi T, Xu J, and Dulac C. A functional circuit underlying male sexual behaviour in the female mouse brain. *Nature* 448: 1009-1014, 2007.
Konishi M. From central pattern generator to sensory template in the evolution of birdsong. *Brain and language* 115: 18-20, 2010.
Lambert L, Dubayle D, Fafouri A, Herzog E, Csaba Z, Dournaud P, El Mestikawy S, and Bernard V. Endocytosis of Activated Muscarinic m2 Receptor (m2R) in Live Mouse Hippocampal Neurons Occurs via a Clathrin-Dependent Pathway. *Frontiers in cellular neuroscience* 12: 450, 2018.
Lawton KJ, Perry WM, Yamaguchi A, and Zornik E. Motor Neurons Tune Premotor Activity in a Vertebrate Central Pattern Generator. *J Neurosci* 37: 3264-3275, 2017.
Mallios VJ, Lydic R, and Baghdoyan HA. Muscarinic receptor subtypes are differentially distributed across brain stem respiratory nuclei. *The American journal of physiology* 268: L941-949, 1995.

Marder E, and Bucher D. Central pattern generators and the control of rhythmic movements. *Current biology : CB* 11: R986-996, 2001.
Meng W, Wang S, Yao L, Zhang N, and Li D. Muscarinic Receptors Are Responsible for the Cholinergic Modulation of Projection Neurons in the Song Production Brain Nucleus RA of Zebra Finches. *Frontiers in cellular neuroscience* 11: 51, 2017.
Mutolo D, Cinelli E, Bongianni F, and Pantaleo T. Identification of a cholinergic modulatory and rhythmogenic mechanism within the lamprey respiratory network. *J Neurosci* 31: 13323-13332, 2011.
Potter KA, Bose T, and Yamaguchi A. Androgen-induced vocal transformation in adult female African clawed frogs. *J Neurophysiol* 94: 415-428, 2005.
Raghuraman S, Garcia AJ, Anderson TM, Twede VD, Curtice KJ, Chase K, Ramirez JM, Olivera BM, and Teichert RW. Defining modulatory inputs into CNS neuronal subclasses by functional pharmacological profiling. *Proceedings of the National Academy of Sciences of the United States of America* 111: 6449-6454, 2014.
Ramirez JM, Severs LJ, Ramirez SC, and Agosto-Marlin IM. Advances in cellular and integrative control of oxygen homeostasis within the central nervous system. *The Journal of physiology* 596: 3043-3065, 2018.
Rezaval C, Pattnaik S, Pavlou HJ, Nojima T, Bruggemeier B, D'Souza LAD, Dweck HKM, and Goodwin SF. Activation of Latent Courtship Circuitry in the Brain of Drosophila Females Induces Male-like Behaviors. *Current biology : CB* 26: 2508-2515, 2016.
Rhodes HJ, Yu HJ, and Yamaguchi A. Xenopus vocalizations are controlled by a sexually differentiated hindbrain central pattern generator. *J Neurosci* 27: 1485-1497, 2007.
Rubsamen R, and Betz M. Control of echolocation pulses by neurons of the nucleus ambiguus in the rufous horseshoe bat, Rhinolophus rouxi. I. Single unit recordings in the ventral motor nucleus of the laryngeal nerves in spontaneously vocalizing bats. *Journal of comparative physiology A, Sensory, neural, and behavioral physiology* 159: 675-687, 1986.
Schmidt MF, McLean J, and Goller F. Breathing and vocal control: the respiratory system as both a driver and a target of telencephalic vocal motor circuits in songbirds. *Experimental physiology* 97: 455-461, 2012.
Shao XM, and Feldman JL. Central cholinergic regulation of respiration: nicotinic receptors. *Acta pharmacologica Sinica* 30: 761-770, 2009.
Shao XM, Tan W, Xiu J, Puskar N, Fonck C, Lester HA, and Feldman JL. Alpha4* nicotinic receptors in preBotzinger complex mediate cholinergic/nicotinic modulation of respiratory rhythm. *J Neurosci* 28: 519-528, 2008.
Silkstone M, and Brudzynski SM. Dissimilar interaction between dopaminergic and cholinergic systems in the initiation of emission of 50-kHz and 22-kHz vocalizations. *Pharmacology, biochemistry, and behavior* 188: 172815, 2020.
Sweeney LB, and Kelley DB. Harnessing vocal patterns for social communication. *Current opinion in neurobiology* 28: 34-41, 2014.
Team RC. R: A language and environment for statistical computing. . Vienna, Austria: R Foundation for Statistical Computing, 2013.
Teichert RW, Memon T, Aman JW, and Olivera BM. Using constellation pharmacology to define comprehensively a somatosensory neuronal subclass. *Proceedings of the National Academy of Sciences of the United States of America* 111: 2319-2324, 2014.

Teichert RW, Raghuraman S, Memon T, Cox JL, Foulkes T, Rivier JE, and Olivera BM. Characterization of two neuronal subclasses through constellation pharmacology. *Proceedings of the National Academy of Sciences of the United States of America* 109: 12758-12763, 2012.
Wan M, Zhang W, Tian Y, Xu C, Xu T, Liu J, and Zhang R. Unraveling a molecular determinant for clathrin-independent internalization of the M2 muscarinic acetylcholine receptor. *Scientific reports* 5: 11408, 2015.
Yamaguchi A, Kaczmarek LK, and Kelley DB. Functional specialization of male and female vocal motoneurons. *J Neurosci* 23: 11568-11576, 2003.
Yu HJ, and Yamaguchi A. Endogenous serotonin acts on 5-HT2C-like receptors in key vocal areas of the brain stem to initiate vocalizations in Xenopus laevis. *J Neurophysiol* 103: 648-658, 2010.
Zornik E, and Yamaguchi A. Coding rate and duration of vocalizations of the frog, Xenopus laevis. *J Neurosci* 32: 12102-12114, 2012.

Figure Legends

Figure 1. Images of dissociated cells obtained from parabrachial (PB) nucleus of male *X. laevis*. A. Bright-field image of dissociated cells from PB. B. Pseudocolored ratiometric calcium image acquired at resting condition. Note that many cells are blue in color indicating low cytoplasmic [Ca^{2+}]. C. Pseudocolored ratiometric calcium image during application of 30mM KCl. Note that many cells are in green to yellow color indicating higher cytoplasmic [Ca^{2+}].

Figure 2. Example calcium imaging traces from two parabrachial neurons. The x-axis and y-axis indicate the time, a relative measurement of cytoplasmic [Ca^{2+}], respectively. Arrows indicate the time at which pharmacological agents were applied, and the black horizontal bar indicates the time during which cells were incubated with GABA and glycine. A. Two traces that exemplify

753 neurons that show consistent response to a high concentration of $[K^+]_o$, but do not respond to any
754 other ligands applied. These neurons belong to class B-III (Table 2). B. Two traces that
755 exemplify neurons that respond to the application of NMDA, SP, ACh, ATP, and GABA with
756 glycine, but not to the application of 5-HT. The neurons belong to pFTN-IV (Table 2). In A, the
757 peak $[Ca^{2+}]_i$ transient amplitude in response to the second $[K^+]_o$ (preceded by incubation with
758 GABA and glycine) is the same as those in response to the first and third $[K^+]_o$, whereas, in B,
759 the second application of $[K^+]_o$ elicits reduced responses compared to the first and third $[K^+]_o$
760 applications. These response profiles are taken as evidence for the lack (A) or presence (B) of
761 the functional expression of the receptors for GABA and/or glycine, respectively.
762
763 Figure 3. Characteristics of class A and class B neurons. A: a photomicrograph of
764 representative class A (left, larger) and B (right, smaller) neurons. B: Two example calcium
765 imaging traces of class A neurons. The x- and y-axis indicate the time and a relative
766 measurement of cytoplasmic $[Ca^{2+}]$, respectively. Arrows indicate the time at which
767 pharmacological agents were applied, and the black horizontal bar indicates the time during
768 which cells were incubated with GABA and glycine. Note that the peak amplitude of $[Ca^{2+}]$
769 transients in response to a high concentration of $[K^+]_o$ is smaller compared to the peak amplitude
770 in response to ATP, and this is one of the criteria we used to define class A neurons. The top and
771 bottom traces are examples of class A-I and class A-II, respectively (Table 2). Many class A
772 neurons show intrinsic $[Ca^{2+}]$ oscillation in the absence of any ligands, as evidence in these
773 traces, for reasons that are not clear. C: Two example calcium imaging traces of class B neurons.
774 The top and bottom traces are examples of pFTN-II and B-III neurons, respectively. Note that

775 the peak amplitude of [Ca^{2+}] transients in response to a repeated application of a high
776 concentration of K^+ is consistently higher than those in response to other ligands.
777
778 Figure 4. Example calcium imaging traces of putative FTN (pFTN-) I through IV. The x- and y-
779 axis indicate the time and a relative measurement of cytoplasmic [Ca^{2+}], respectively. Arrows
780 indicate the time at which pharmacological agents were applied, and the black horizontal bar
781 indicates the time during which cells were incubated with GABA and glycine. A. Two example
782 calcium imaging traces from pFTN-I. These neurons respond to NMDA and GABA with glycine
783 application, but not to ACh or SP. B. Two example calcium imaging traces of pFTN-II. These
784 neurons respond to NMDA, GABA with glycine, and SP. C. Two example calcium imaging
785 traces of pFTN-III. These neurons respond to NMDA, GABA with glycine, and ACh application.
786 D. Two example of calcium imaging traces of pFTN-IV. These neurons respond to NMDA,
787 GABA with glycine, SP, and ACh application.
788
789 Figure 5. Responses of Fast Trill Neurons (FTNs) to acetylcholine (ACh) and substance P (SP).
790 A. Top trace: Recordings obtained from the laryngeal nerve of isolated brain preparation.
791 Bottom trace: membrane potential recorded from the FTN during fictive vocal production.
792 Green frame shows fast trill and blue frame show slow trills, two distinct phases of the
793 advertisement calls of male *X. laevis*. The long-lasting depolarization of the membrane potential
794 and the repetitive firing during the fast trill is a signature membrane potential activity of the
795 FTNs. B. Example trace of the membrane potential of the neuron (green plot in C) in response
796 to the 10-minutes bath application of acetylcholine (left) and substance P (right). The parts of
797 the traces with artifact associated with the ligand application and other random noises are

798 removed. C. The membrane potentials (average of 30 seconds) of four FTNs before, during, and
799 after the application of ACh (left) and SP (right). Prior to the experiment, TTX was applied to
800 the whole-brain preparation to block all synaptic transmission mediated by action potentials.
801 Each color indicates data obtained from each neuron (n=4). Based on the response profile, the
802 blue neuron is pFTN-III, and the purple, red, and green neurons are pFTN-IV.
803
804 Figure 6. A role of substance P and acetylcholine in the parabrachial (PB) nucleus in the
805 production of fictive vocalizations. A: Example injection site of agonists and antagonists shown
806 in a horizontal section of the brain of *X. laevis*. The top and the bottom of the images are the
807 rostral and the caudal edge of the tissue, respectively, and the dotted white line indicates the
808 midline. Neurotrace staining is in green, and injection sites are shown in red. A white rectangle
809 area on the left image is enlarged on the right. N.I, nucleus isthmi; N.V., cranial nerve V; OT,
810 optic tectum; PB, parabrachial nucleus; V.IV, fourth ventricle. For all the laryngeal nerve
811 recording traces shown in C through F, the y-axis is the same for before (5-HT), during
812 (pharmacological agents), and after (wash, saline, DMSO) the drug injection for each brain, even
813 though the noise is increased in some cases. B. Summary of the pharmacological experiments.
814 "atr/tbc"; the cocktail of atropine and tubocurarine, "n"; sample size, "% brain sang with
815 ligands"; the proportion of brains that generated fictive vocalizations (including fast and/or slow
816 trills) in response to the ligand injection or bath application, "% brain sang after washout"; the
817 proportion of the brain that sang in response to the application of 5-HT after the target ligands
818 were washed out for one to four hours. C. Laryngeal nerve recordings in response to the
819 bilateral injection of ACh into PB (n=6). Left, fictive advertisement calls recorded from the
820 laryngeal nerve in response to the bath application of 5-HT one hour before ACh injection.

Middle, laryngeal nerve recordings obtained in response to ACh injected into PBs. Right, laryngeal nerve recordings obtained in response to 5-HT application one hour after ACh was washed out of the bath. D. Laryngeal nerve recordings in response to the bilateral injection of SP into PBs (n=4). D1, D2, and D3 show three different responses observed from four brains injected with SP into PB. Left, fictive advertisement calls recorded from the laryngeal nerve in response to the bath application of 5-HT one hour before SP injection. Right for D1 and D2, middle for D3, laryngeal nerve recordings after SP was injected bilaterally into the PBs. D3. Right, fictive advertisement calls recorded from the laryngeal nerve in response to the bath application of 5HT after a one-hour wash of SP injection into PB. E. Laryngeal nerve recordings in response to the bilateral injection of atropine and tubocurarine followed by 5-HT (n=5). Left, fictive advertisement calls recorded from the laryngeal nerve in response to the bath application of 5-HT. Middle, laryngeal nerve recordings obtained when atropine and tubocurarine were injected bilaterally into PBs immediately followed by the bath application of 5-HT. Right, laryngeal nerve recordings obtained when the vehicle (saline) was bilaterally injected into PB immediately followed by bath application of 5-HT. F. Laryngeal nerve recordings in response to the bilateral injection of aprepitant immediately followed by 5-HT application (n=3). Left, fictive advertisement calls recorded from the laryngeal nerve in response to the bath application of 5-HT. Middle, laryngeal nerve recordings obtained when aprepitant was injected bilaterally into PB immediately followed by the bath application of 5-HT. Right, laryngeal nerve recordings obtained when the vehicle (10% DMSO in saline) were bilaterally injected into PB followed by bath application of 5-HT. G. Peak amplitude and instantaneous frequency of the compound action potentials (CAPs) plotted against CAP order for fictive fast trills obtained from brains before, during, and after aprepitant injection into the PBs (data shown

844 in F). Gray traces are individual calls (n = 3 to 10 calls per animal per treatment), and the black
845 traces are average for each animal for each experimental condition. Note that the CAP
846 amplitude and instantaneous frequency show a progressive increase during fast trills before (5-
847 HT, left) and after (DMSO, 5-HT, right), but not during bilateral injection of aprepitant into PBs
848 (middle).
849
850 Figure 7. Example calcium imaging traces of putative FTN (pFTN-) I through IV obtained from
851 female parabrachial nucleus. The x- and y-axis indicate the time and a relative measurement of
852 cytoplasmic [Ca^{2+}], respectively. Arrows indicate the time at which pharmacological agents
853 were applied, and the black horizontal bar indicates the time during which cells were incubated
854 with GABA and glycine.
855
856 Figure 8. Frequency histogram of 12 subclasses of parabrachial neurons of adult male (n = 8) and
857 female (n = 4) *X. laevis*. Each bar indicates the average and standard error. Although males and
858 females produce sexually distinct vocalizations, all 12 subclasses of PB neurons found in males
859 are also found in females at a similar frequency. Mann-Whitney U test, Z statistics, and p-value
860 are shown under the histogram for each cell subclass. Note that none of the comparisons are
861 statistically significant.

862

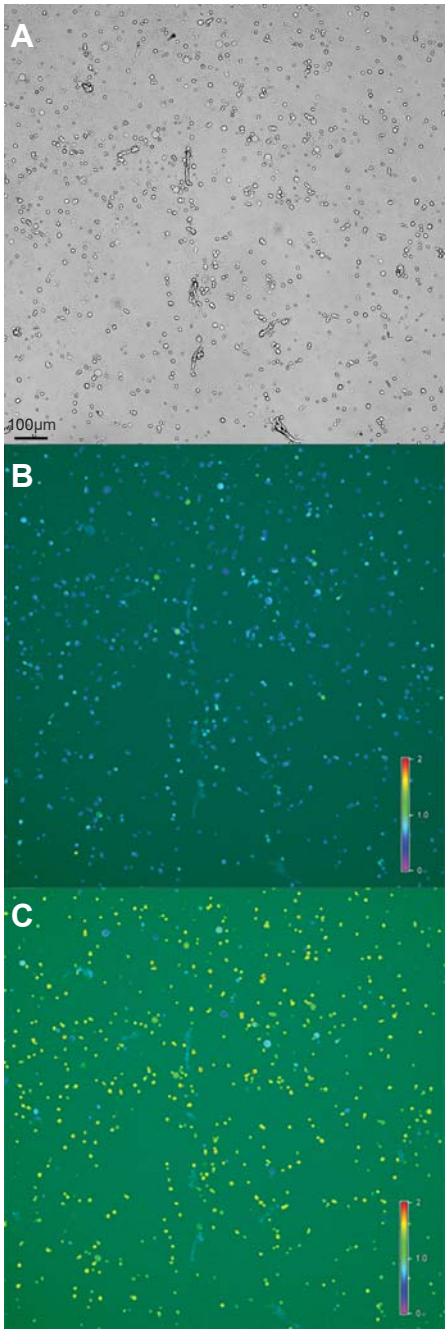

Figure 1

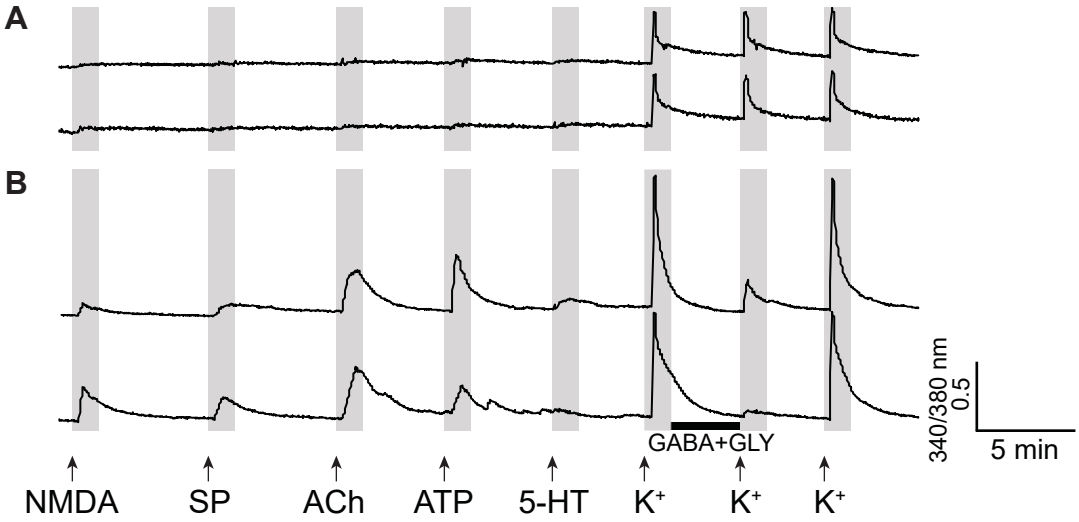

Figure 2

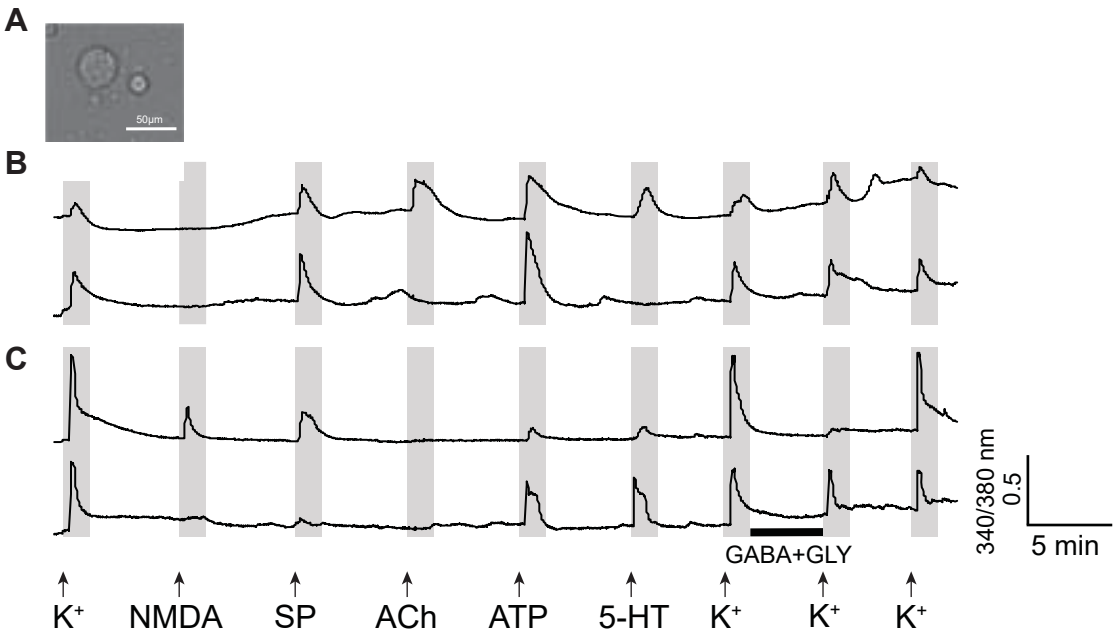

Figure 3

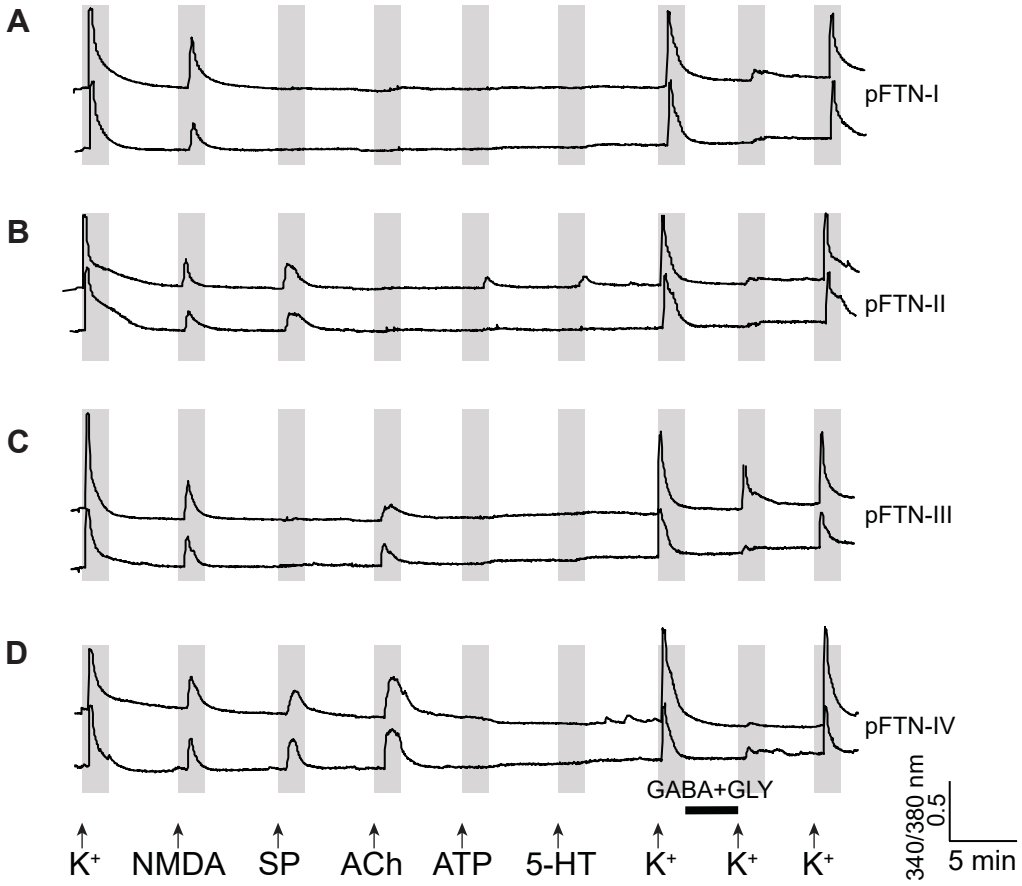

Figure 4

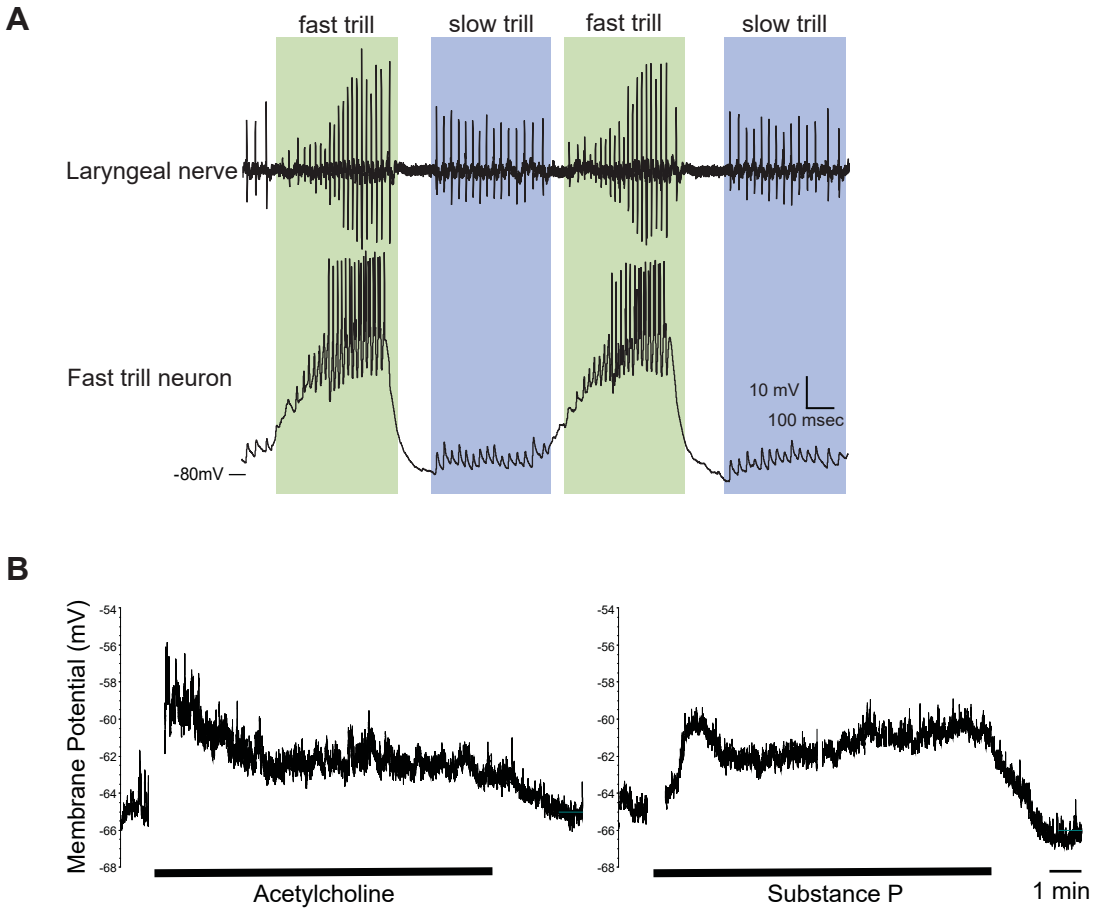

Figure 5

A.

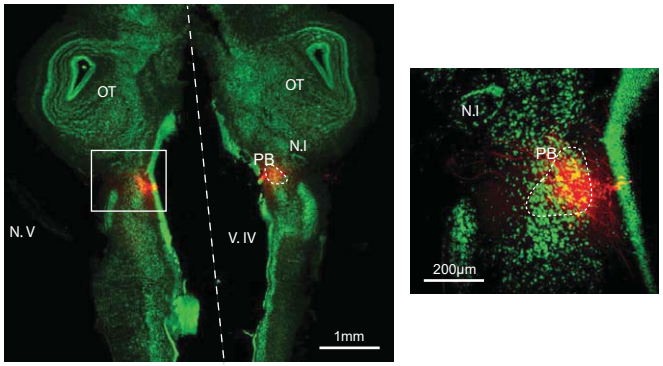

B.

Pharmacological agents	Delivery method	n	% brain sang with ligands	% brain sang after washout
ACh	PB injection	8	0	0
SP	PB injection	4	50	100
Saline	PB injection	6	n.a.	100
ACh	bath application	3	0	100
SP	bath application	7	57	100
atr/tbc + 5HT	PB injection	5	0	100
aprepitant + 5HT	PB injection	3	100	100

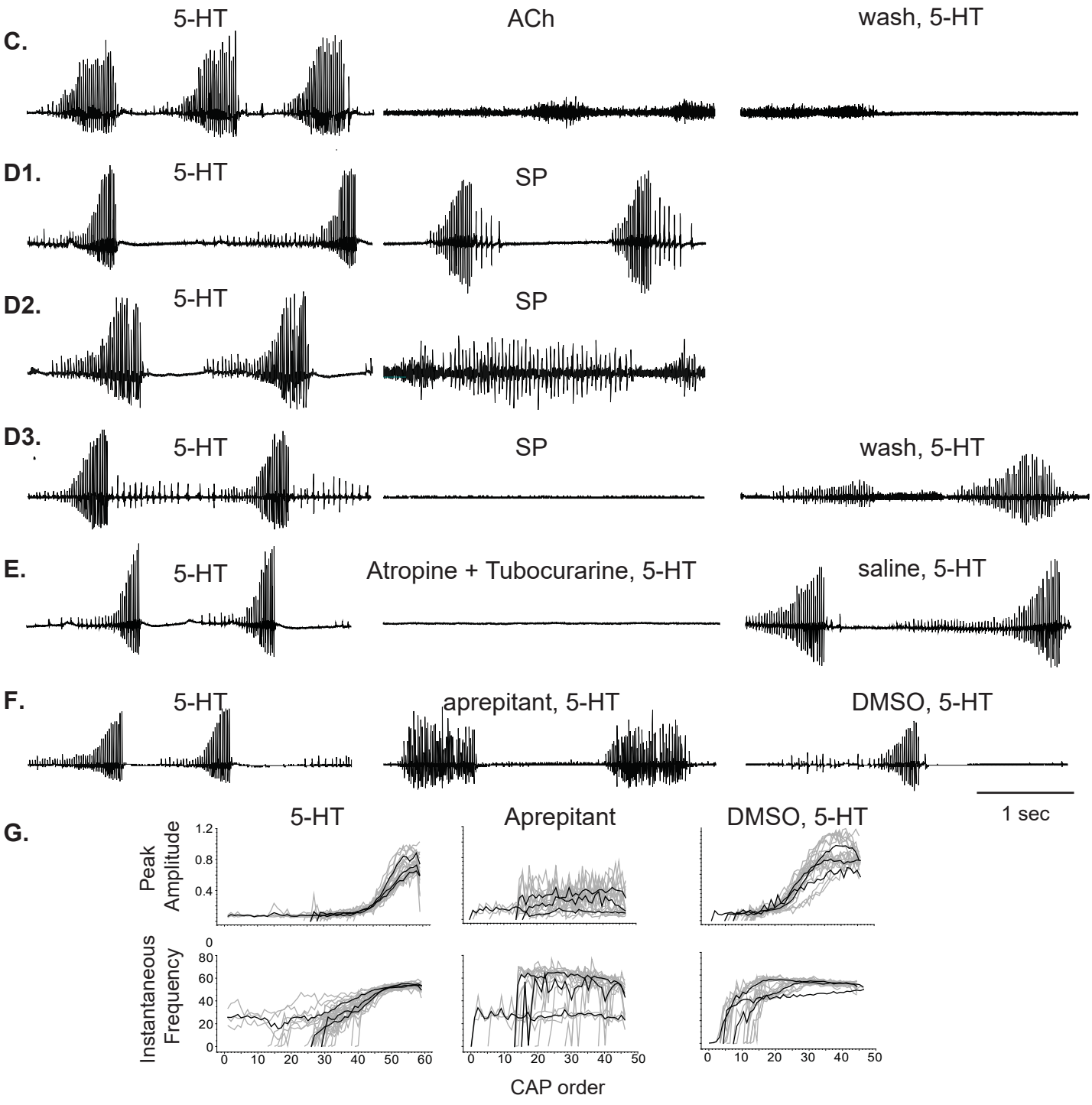

Figure 6

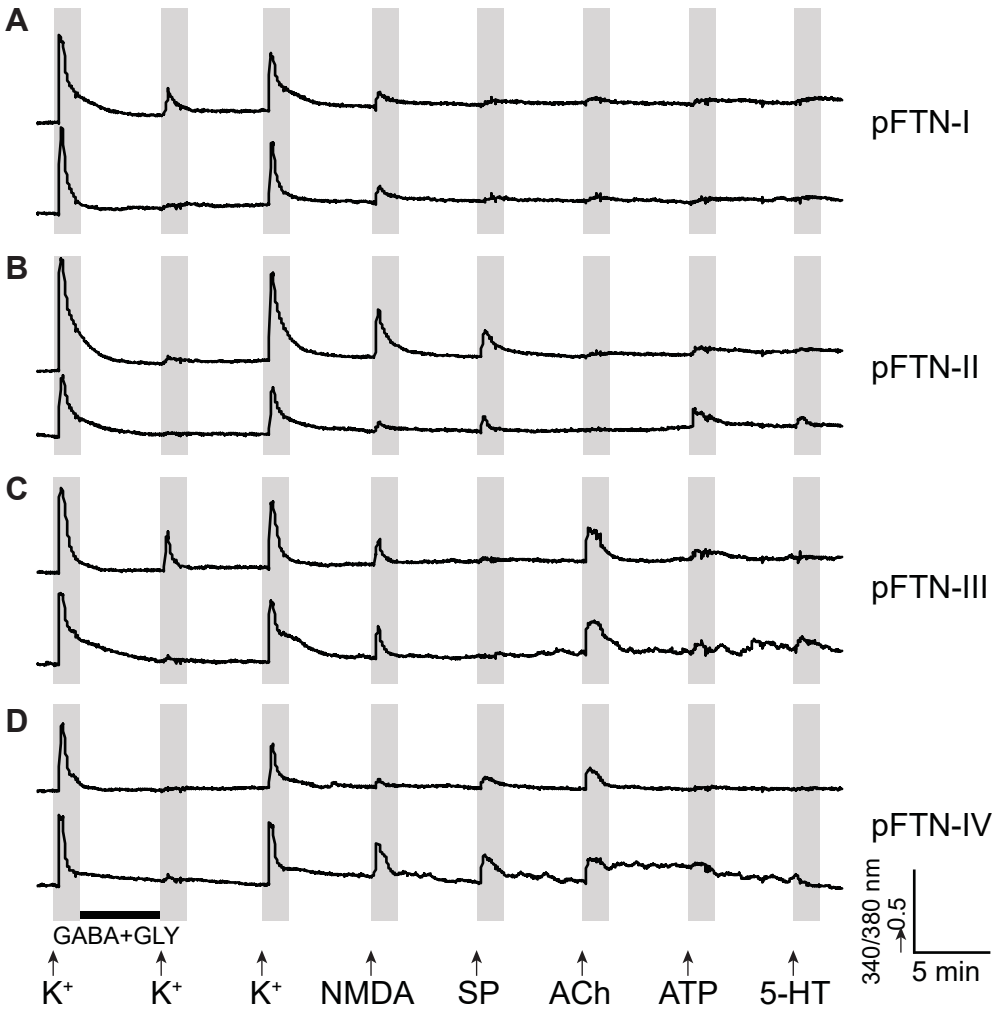

Figure 7

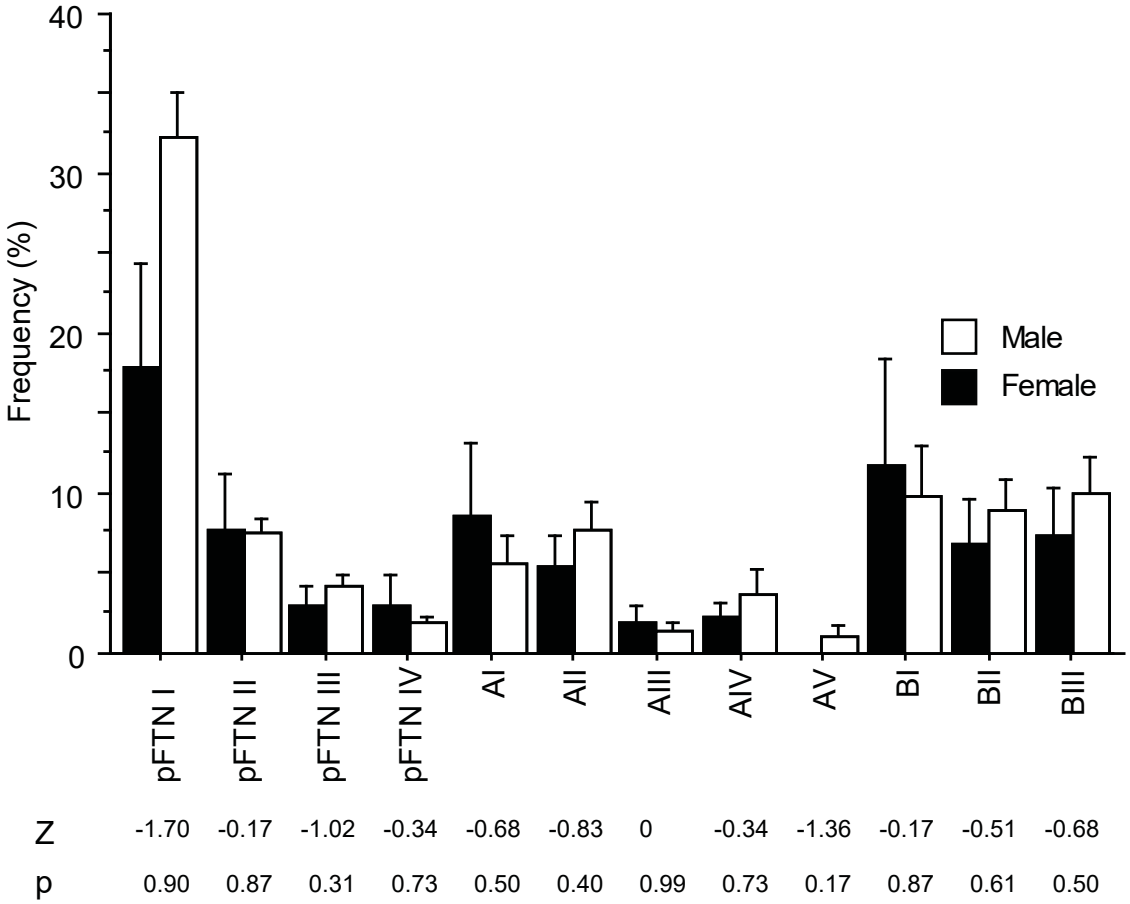

	pFTN I	pFTN II	pFTN III	pFTN IV	AI	AII	AIII	AIV	AV	BI	BII	BIII
Z	-1.70	-0.17	-1.02	-0.34	-0.68	-0.83	0	-0.34	-1.36	-0.17	-0.51	-0.68
p	0.90	0.87	0.31	0.73	0.50	0.40	0.99	0.73	0.17	0.87	0.61	0.50

Figure 8

Abbreviation	Pharmacology Agent	Working concentration	Target Receptor
NMDA	N-methyl-D-aspartate	200μM	NMDA-receptor
SP	Substance P	1μM	Neurokinin-1-receptor
Ach	Acetylcholine	1mM	Acetylcholine-receptor
ATP	Adenosine 5’ triphosphate	20μM	Purinergic-receptor
5-HT	Serotonin	25μM	5-HT-receptor
GABA	Gamma-aminobutyric acid	1mM	GABAergic-receptor
Gly	Glycine	1mM	Glycinergic-receptor
D-ser	D-serine	20μM	NMDA-receptor
H	Histamine	50μM	Histamine-receptor
Br	Bradykinin	10μM	Bradykinin-receptor

Table 1. Abbreviation and working concentration of pharmacological agents

Cell Types	Classification Criteria	Total # cells	% cells/animal (mean + SE)	% response to pharmacological agents (mean + SE)					
				NMDA	SP	ACh	ATP	GABA	5-HT
Neurons	+ [K^+]	11,074	85 ± 7	69±0.4	32±0.4	29±0.4	38±0.5	58±0.5	28±0.4
Class A K^+ amp (0.18±0.003) Cell area (214±1.7μm^2)	K^+amp<ATP amp >100 μm^2	1,902	17±3	18±0.9	49±1.1	89±0.7	100	8±0.6	87±0.8
A-I	+[SP, ATP,ACh,5-HT]	879	9±2	20±1	100	100	100	6±1	100
A-II	+[SP,ATP] -[ACh,5-HT]	59	1±0	59±6	100	0	100	29±6	0
A-III	+[ATP,ACh,5-HT] -[SP]	636	6±1	12±1	0	100	100	6±1	100
A-IV	+[ATP,5-HT] -[SP,ACh]	142	2±0	20±3	0	0	100	15±3	100
A-V	+[ATP] -[SP,ACh,5-HT]	186	2±1	10±2	0	100	100	10±2	0
Class B K^+ amp (0.61±0.002) Cell area (74±0.28μm^2)	<150 μm^2	9,172	68±4	80±0.4	28±0.5	17±0.4	25±0.5	68±0.5	15±0.4
pFTN-I	+[NMDA,GABA] -[SP,ACh]	3,245	30±3	100	0	0	14±1	100	9±1
pFTN-II	+[NMDA,GABA,SP] -[ACh]	1,271	11±1	100	100	0	36±1	100	16±2
pFTN-III	+[NMDA,GABA,AC] -[SP]	550	5±1	100	0	100	19±2	100	15±2
pFTN-IV	+[NMDA,GABA,SP,ACh]	400	3±1	100	100	100	42±2	100	20±1
B-I	+[NMDA] -[GABA]	1,882	14±4	100	29±1	19±1	26±1	0	17±1
B-II	+[GABA] -[NMDA]	783	7±2	0	16±1	6±1	20±1	100	15±1
B-III	-[NMDA,GABA]	1,041	10±2	0	23±1	16±1	51±2	0	32±1
Non-neuronal cells	- [K^+]	2,011	15±3	33±5	32±3	42±4	40±3	NA	22±3

Table 2. The classification of cell types obtained from the parabrachial nucleus of male Xenopus laevis. "Classification criteria" describes characteristics used to define classes and subclasses of cells. +[ ] and -[ ] indicates the presence and absence of Ca^{2+} responses to the pharmacological agents contained in the brackets, respectively. "Total # cells" indicate all the cells that were categorized into classes of neurons across 8 animals. "% cells/animal" indicates mean ± standard error (SE) of the proportion of cells that were categorized into each class within each animal. "% responses to pharmacological agents" show mean U SE of the proportion of neurons that responded to each ligand within each class and subclass. The threshold criteria to define the presence and absence of responses are described in the Materials and Methods section. Asterisks in the first column indicate mean ± SE of the peak Ca amplitude in response to a high K^+ application and the surface area for Class A and Class B neurons.